

We are IntechOpen, the world's leading publisher of Open Access books Built by scientists, for scientists

4,800

Open access books available

122,000

International authors and editors

135M

Downloads

Our authors are among the

154

Countries delivered to

TOP 1%

most cited scientists

12.2%

Contributors from top 500 universities



WEB OF SCIENCE™

Selection of our books indexed in the Book Citation Index
in Web of Science™ Core Collection (BKCI)

Interested in publishing with us?
Contact book.department@intechopen.com

Numbers displayed above are based on latest data collected.
For more information visit www.intechopen.com



Static and Dynamic Photovoltaic Cell/Module Parameters Identification

Sid-Ali Blaifi and Bilal Taghezouit

Abstract

The accurate parameters extraction is an important step to obtain a robust PV outputs forecasting for static or dynamic modes. For these aims, several approaches have been proposed for photovoltaic (PV) cell modeling including electrical circuit-based model, empirical models, and non-parametrical models. Moreover, numerous parameter extraction methods have been introduced in the literature depending on the proposed model and the operating mode. These methods can be classified into two main approaches including automatic numerical and analytical approaches. These approaches are commonly applied in the static mode, whereas they can be employed for dynamic parameters extraction. In this chapter, as a first stage, the static parameters extraction for both single and double diodes models is exposed wherein Genetic Algorithm and outdoor measurements are considered for fixed irradiation and temperature. In the second stage, a dynamic parameters extraction is carried out using Levenberg-Marquardt algorithm, where 1 day profile outdoor measurement is considered. After that, the robustness of the proposed approaches is evaluated and the parameters obtained by the static method and that given by the dynamic technique are compared. The test is carried out using 3 days with different weather conditions profiles. The obtained results show that the parameters extraction by dynamic techniques gives satisfactory performances in terms of agreement with the real data.

Keywords: photovoltaic module, static parameters extraction, dynamic parameters extraction, empirical model, electrical model

1. Introduction

The increasing development of PV technologies brought out their potential to provide the energy abundance across the world. Hence, they have been interested by several research groups in the purpose to improve their behavior and extend their life-time. Meanwhile, giving an accurate forecasting of the PV outputs behavior has been always a real issue related to their nonlinearity. Two modes can characterize the PV module in terms of modeling, the first one is the static mode wherein the obtained model is characterized and validated for fixed weather conditions (irradiation and temperature), while the second is the dynamic mode where the validation is carried out using variable weather conditions. In this context, several models of the PV cell/module have been introduced in the

literature based mainly on several approaches including electrical, empirical, and non-parametrical modeling. For the non-parametrical models, two approaches are introduced namely, Artificial Neural Network (ANN) and Neuron-Fuzzy based models. The accuracy and the robustness of these approaches rely strongly on the richness of the training dataset in terms of scenarios. Neuron-Fuzzy techniques has been used to predict cell short-circuit current and open-circuit voltage for the static representation [1]. The ANN-based technique is introduced to model the PV array power for the embedded systems implementation [2]. This technique has been tested for dynamic mode dealing [3]. The ANN technique is also used for the prediction of the PV cell/module voltage directed to amorphous silicon PV technology wherein the obtained network has been tested by real dynamic data [4].

In the empirical or the analytical approaches, several models have been proposed to estimate accurately both static and dynamic modes of PV cell/modules. An analytical model is proposed by [5] based on manufacturer characteristic. This model provides acceptable results for both static and dynamic working. Another model has been introduced by Sandia National Laboratory [6], which is widely employed for PV cell/model forecasting especially for the large-scale arrays. Other empirical models have been proposed in order to estimate the PV array power under uniform shading [7, 8].

In the electrical approaches, two models widely prevail owing to their simplicity based on equivalent circuits namely: single (SDM) and double (DDM) diodes-based models. These models can deal with both static and dynamic modes with an acceptable accuracy. Besides, several enhancements have been introduced in these models to minimize parameters number and give more simplicity [9, 10]. The expressions of both photo-generation and diode saturation currents have been improved to give more accuracy in the dynamic working [11].

All models possess unknown parameters, which should be identified according to the module used in the practice. For this end, numerous approaches have been introduced in the literature including analytical and automatic numerical methods. The analytical methods usually rely on specific points on the I-V curve and on some value given by manufacturer. However, a significant error can be engendered if one of more of selected points is incorrect [12].

Owing to their adequate results, automatic numerical methods are prevail in PV models parameters extraction either through the use of deterministic algorithms such as: Newton model modified with Levenberg [13], Levenberg-Marquardt [14], Simulated Annealing algorithm (SA) [15], Pattern Search (PS) [16], Nelder-Mead Simplex algorithm (NMS) [17], and hybrid Nelder-Mead and modified particle swarm optimization [18] or by introducing metaheuristic algorithms such as: Genetic Algorithms (GA) [19], Particle Swarm Optimization (PSO) [20–26], Cuckoo Search (CS) [27], Artificial Bee Colony (ABC) [26, 28], and Artificial Bee Swarm (ABS) [29]. Moreover, other algorithms have been introduced like (FPA) [30, 31], hybrid Bee Pollinator Flower Pollination Algorithm (BPFPA) [31, 32], Harmony Search (HS) [33], Artificial Fish Swarm Algorithm (AFSA) [34], and other algorithms. The majority of the aforementioned algorithms have been applied for static parameters extraction.

Numerical algorithms have been also applied for dynamic parameters extraction wherein the identification process is carried out using variables weather conditions [35, 36].

In this chapter, modeling and parameters extraction of PV cell/module are detailed. Where, comparison study among three models by applying static and dynamic identification using out-door measurement.

2. PV cell/module modeling

The PV cell presents outputs variation, which depends on weather conditions namely, irradiation and temperature. As illustrated in **Figure 1**, for load variation from open circuit to short circuit, the PV cell shows nonlinear characteristic that possess a maximum point of power. For an optimal working, the load should be adapted at this point. In this section, three PV cell models will be employed and improved using automatic parameters extraction namely: the empirical Sandia model and both single and double diodes electrical models.

2.1 Sandia model

This empirical model given by SANDIA National Laboratories provides relatively accurate dynamic forecast for PV cell/module by describing the thermal, the electrical, and the optical characteristics. Also, this model can be destined for any technology and can be adapted with any scale of PV arrays. Furthermore, its simplicity can qualify it to be used for real-time online prediction. Expressions (1)–(4) describe the variation of I_{mp} , V_{mp} , and P_{mp} , respectively.

$$I_{mp} = I_{mp_STC} (C_0 E_e + C_1 E_e^2) (1 + \alpha_{mp} (T - T_{STC})) \quad (1)$$

$$V_{mp} = V_{mp_STC} + C_2 N_s \times \delta(T) \times \ln(E_e) + C_3 N_s (\delta(T) \ln(E_e))^2 + \beta_{mp} (T - T_{STC}) \quad (2)$$

$$\delta(T) = \frac{n \times k \times (T + 273.15)}{q} \quad (3)$$

$$P_{mp} = I_{mp} \times V_{mp} \quad (4)$$

where, C_{0-3} are empirical parameters to be identified, I_{mp_STC} , V_{mp_STC} are the current and the voltage in the maximum power point under standard test condition, E_e is the effective irradiation, K is the Boltzmann constant, q is the electron charge, $\delta(T)$ is the thermal voltage, α_{mp} and β_{mp} are, respectively, the current and the voltage temperature coefficient [36].

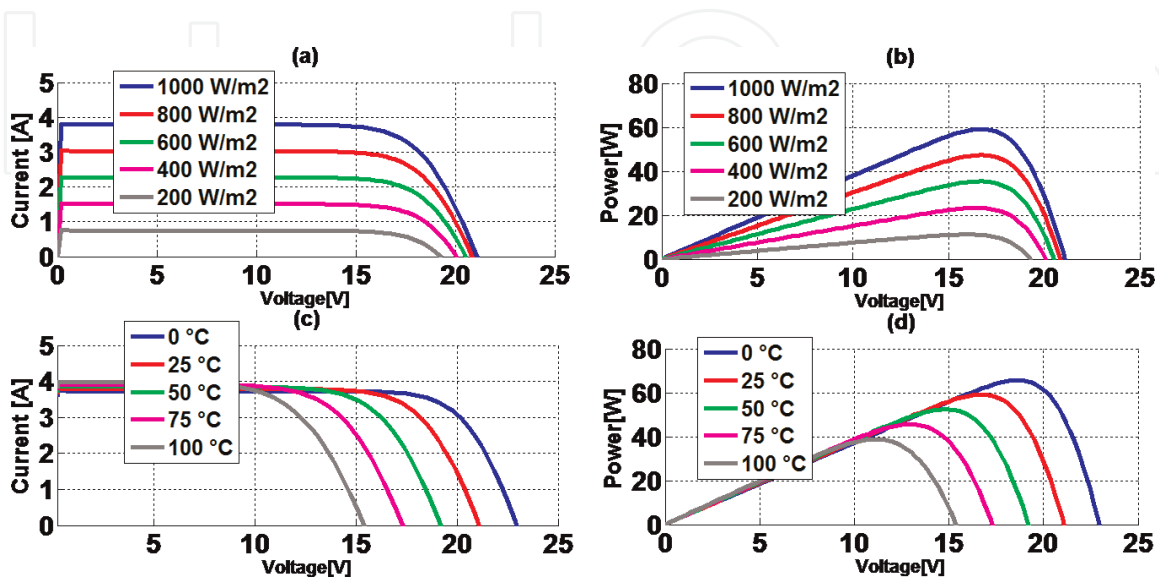


Figure 1. PV characteristic for different irradiation and temperature. (a) Current versus voltage for different irradiation; (b) Power versus voltage for different irradiation; (c) Current versus voltage for different temperature; (d) Power versus voltage for different temperature.

2.2 Single diode based model (SDM)

This physical model is based on the electrical approach illustrated in **Figure 2** wherein the PV cell is composed of: a photo-generation current source and a diode while joule losses are represented by two serial and parallel resistors.

From this electrical representation, expression (5) and (6) can be obtained to describe the evolution of both current and voltage. The output current is expressed as a sum of the photo-generation current I_{ph} , the diode current I_d , and the shunt current I_{sh} .

$$I = I_{ph} - I_d - I_{sh} \quad (5)$$

$$I_d = I_0 \left[\exp \left(\frac{q(V + R_s I)}{nKT} \right) - 1 \right] \quad (6)$$

$$I_{sh} = \frac{V + R_s I}{R_{sh}} \quad (7)$$

where, K is the constant of Boltzmann, q is the electron charge, T is the cell temperature, n is the diode ideality factor, and I_0 is the current saturation due to diffusion and recombination.

After the substitution of Eqs. (6) and (7) in (5), the following expression is obtained:

$$I = I_{ph} - I_0 \left[\exp \left(\frac{q(V + R_s I)}{nKT} \right) - 1 \right] - \frac{V + R_s I}{R_{sh}} \quad (8)$$

R_s , R_{sh} , and n are parameters to be identified in the static study and can be adjusted in the dynamic study.

Diode saturation current I_0 is expressed in Eq. (9) function of the cell temperature and the energy band-gap [11].

$$I_0 = \frac{I_{sc} \times T^3 \times \exp \left(-\frac{q \times E_g}{KT} \right)}{\left(\exp \left(\frac{q \times V_{oc}}{nKT_r} \right) - 1 \right) \times T_r^3 \times \exp \left(-\frac{q \cdot E_{gr}}{KT_r} \right)} \quad (9)$$

Eq. (10) describes the evolution of the energy band-gap E_g as function of the cell temperature.

$$E_g = E_{g0} - \left(\frac{\alpha \times T^2}{\beta + T} \right) \quad (10)$$

where E_{g0} and E_{gr} are the energy band-gap of the silicon at 0°C and at the reference temperature T_r , respectively, α and β are constants of the material.

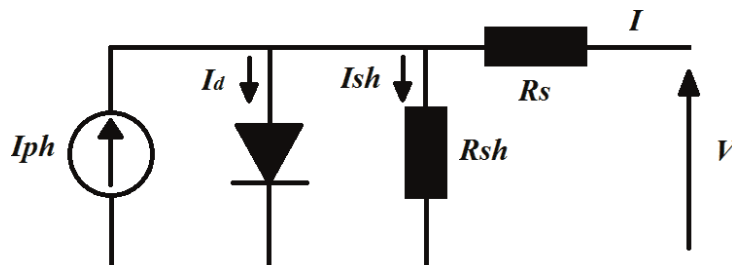


Figure 2.
Single diode equivalent circuit.

The photo-generation current is given by Eq. (11) as a function of the irradiation and the cell temperature.

$$I_{ph} = \frac{G}{1000} [I_{sc} + \mu(T - T_r)] \quad (11)$$

where G is the input irradiation, T is the cell temperature, I_{sc} is the module short-circuit current, and μ is the coefficient temperature/short-circuit current (given by the manufacturer) [11].

E_{g0} , α , β , μ , I_{sc} , and V_{oc} are parameters to be identified in the dynamic study.

2.3 Double diode-based model

From the electrical representation illustrated in **Figure 3**, the PV cell can be represented by a source of current that represents the photo-generation, two diodes and both parallel and serial resistances representing the loss of energy inside the cell.

After applying nodes law, the output current is expressed as sum of: photo-generation current I_{ph} , shunt current I_{sh} and the diodes currents I_{d1} and I_{d2} (Eqs. (12)–(15)).

$$I = I_{ph} - I_{d1} - I_{d2} - I_{sh} \quad (12)$$

$$I_{d1} = I_{01} \left[\exp \left(\frac{q(V + R_s I)}{n_1 K T} \right) - 1 \right] \quad (13)$$

$$I_{d2} = I_{02} \left[\exp \left(\frac{q(V + R_s I)}{n_2 K T} \right) - 1 \right] \quad (14)$$

$$I_{sh} = \frac{V + R_s I}{R_{sh}} \quad (15)$$

In which I_{01-2} are currents saturation of the two diodes that resulted from diffusion and recombination, n_{1-2} are ideally factors.

By substituting Eqs. (13)–(15) in (12), final description of the output current versus the voltage is obtained which is expressed in Eq. (16) [11].

$$I = I_{ph} - I_{01} \left[\exp \left(\frac{q(V + R_s I)}{n_1 K T} \right) - 1 \right] - I_{02} \left[\exp \left(\frac{q(V + R_s I)}{n_2 K T} \right) - 1 \right] - \frac{V + R_s I}{R_{sh}} \quad (16)$$

n_{1-2} and R_s , R_{sh} are parameters which will be identified in the static study and they can be adjusted in the dynamic study.

Eqs. (17) and (18) express the evolution saturation currents of the diodes I_{01-2} versus energy band-gap E_g and cell temperature [11].

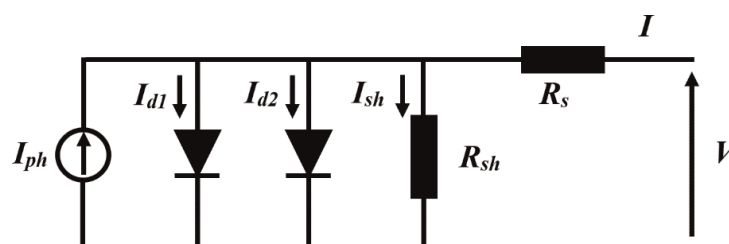


Figure 3.
 Double diodes equivalent circuit.

$$I_{01} = \frac{I_{sc} \times T^3 \times \exp\left(-\frac{q \times E_{g1}}{KT}\right)}{\left(\exp\left(\frac{q \times V_{oc}}{n_1 KT_r}\right) - 1\right) \times T_r^3 \times \exp\left(-\frac{q \times E_{gr}}{KT_r}\right)} \quad (17)$$

$$I_{02} = \frac{I_{sc} \times T^3 \times \exp\left(-\frac{q \times E_{g2}}{KT}\right)}{\left(\exp\left(\frac{q \times V_{oc}}{n_2 KT_r}\right) - 1\right) \times T_r^3 \times \exp\left(-\frac{q \times E_{gr}}{KT_r}\right)} \quad (18)$$

The photo-generation current is represented by the same expression of the single diode model (Eq. (11)).

Parameters E_{g01-2} , α_{1-2} , β_{1-2} , μ , I_{sc} and V_{oc} will be identified in the dynamic study.

3. Static parameters extraction of PV module

For fixed irradiation and temperature, a static parameters extraction will be done to extract five parameters in SDM and seven parameters in DDM. A numerical stochastic optimization algorithm is used in this identification. This algorithm namely, Genetic Algorithm (GA), is employed to minimize the cost function given in Eq. (19) which expresses the root mean square error (RMSE) between the measured PV module $I(v)$ characteristic and that given by the models. For this and, outdoor static measurements have been carried out using the peak measuring device tracer (PVPM 2540C), whose characteristics are illustrated in **Table 1**. This device has been programed to provide both $I(V)$ and $P(V)$ curves of 101 samples per 1 min.

$$RMSE = \sqrt{\frac{1}{N} \sum_{i=1}^N f(V_m, I, P)^2} \quad (19)$$

where I is the simulated current, V_m is the measured voltage, N is the number of sample in $I(V)$ characteristics. The error between the measured and simulated $I(V)$ characteristics for the aforementioned models are expressed in Eqs. (20) and (21).

$$f(V_m, I, P) = I_{ph} - I_0 \left[\exp\left(\frac{q(V_m + R_s I)}{nKT}\right) - 1 \right] - \frac{V_m + R_s I}{R_{sh}} - I_m \quad (20)$$

$$f(V_m, I, P) = I_{ph} - I_{01} \left[\exp\left(\frac{q(V_m + R_s I)}{n_1 KT}\right) - 1 \right] - I_{02} \left[\exp\left(\frac{q(V_m + R_s I)}{n_2 KT}\right) - 1 \right] - \frac{V_m + R_s I}{R_{sh}} - I_m \quad (21)$$

Application	DC voltage	DC current	Temperature	Irradiance	Measuring period single measurement	I-V curve samples
PV modules and small strings	25/50/100/250 V	2/5/10/40 A	-40°C to +120°C with Pt1000	0-1300 (W/m ²) (standard-sensor)	0.02-2 (s)	101

Table 1.
PVPM2540C characteristics.

3.1 Genetic Algorithm

The Genetic Algorithm (GA) is a stochastic algorithm imitated from the biological genetic process used to find an approximate solution for optimization problems. Like in the natural concept, the chromosome is the holder of the genes that the child can probably get from his parents. By analogy, these genes represent the variables (parameters) of the function to be minimized. Five steps can characterize the GA namely, generation of initial population, evaluation of fitness, selection, crossover and mutation [37, 38].

3.1.1 Initial population

The process starts by the generation the initial population of N chromosome coded in binary. Each vector chromosome is formed of group of parameters in which its length M is given in Eq. (22) wherein n is the number of parameters and N_b is the length of the sub-string (number of bits) of each parameter as shown in **Figure 4**. The length of the integer part given by the vector Conv (Eq. (23)) is used to limit the research domain in which, P_i (Eq. (24)) is the parameter value in decimal code [37, 38].

$$M = n \times N_b \quad (22)$$

$$Conv = \left[2^{n_i} 2^{n_i-1} \dots 2^0 2^{-1} \dots 2^{(n_i-N_b+1)} \right] \quad (23)$$

$$P_i = [a_0 a_1 \dots a_{N_b-1}] \times Conv^T \quad (24)$$

3.1.2 Fitness

In this stage, the parameters values that have been randomly generated and decoded in decimal base will be substituted in the cost function to be optimized. The fitness is the solution of the parameters in the RMSE (x) function calculated in Eq. (19). Its value is mathematically expressed in Eq. (23) [37, 38].

$$Fitness(x) = \frac{1}{1 + RMSE(x)} \quad (25)$$

3.1.3 Selection

The chromosomes that will participate as parents to generate a new child are chosen in this step. Any chromosome in the generated population can be chosen however, the individual that presents a good fitness have a high probability. The technique used for the chromosome choice is the roulette wheel illustrated in **Figure 5**, wherein the selection probability P_s , expressed in Eq. (24), is calculated, consists of a cumulative sum of the fitness of each chromosome orderly relative to the sum of all fitness. After that, the process generates a random drawing probability P_r . Hence, the first chromosome corresponds to $P_r < P_s$ is chosen for the next steps (crossover and Mutation).



Figure 4.
Chromosome string.

$$P_s(i) = \frac{\sum_{k=1}^i \text{Fitness}(k)}{\sum_{j=1}^N \text{Fitness}(j)} \quad (26)$$

where, k is an integer counter that varies from 1 to the current chromosome, and j is an integer counter that varies from 1 to the population size N [37, 38].

3.1.4 Crossover

After selecting the chromosomes, the algorithm gives birth to new children by performing a crossover between each two chromosomes. For this end, a drawing probability P_r is generated and compared with the crossover probability P_c (usually high probability). Hence, the parents chromosomes that corresponds to $P_r < P_c$ will be chosen for child generation. If not, the same chromosomes are kept. As illustrated in **Figure 6**, the crossover by point is used wherein the bits after the point randomly chosen are swapped [37, 38].

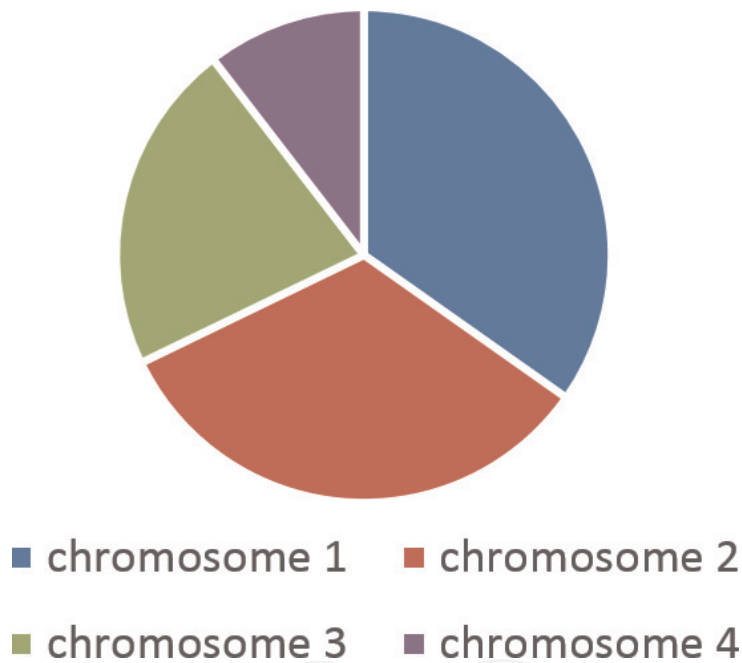


Figure 5.
Roulette wheel example.

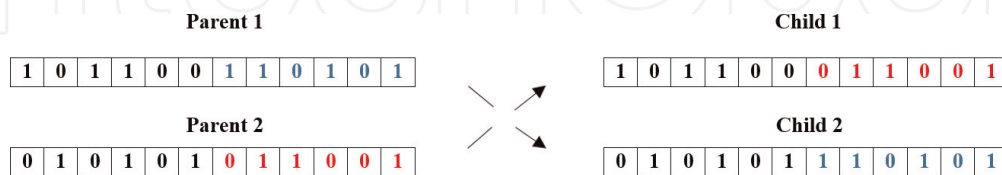


Figure 6.
Crossover process.

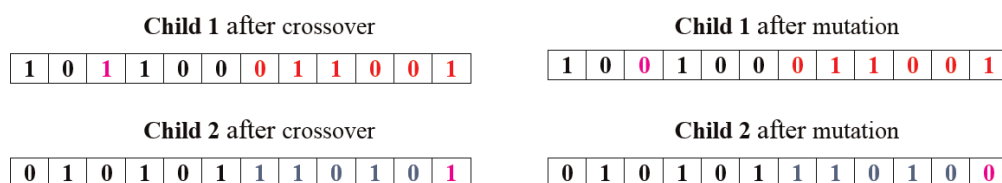


Figure 7.
Mutation process.

3.1.5 Mutation

In this step, the algorithm introduces a change in some characters of the selected chromosomes in order to expand the search space if the initial population does not

Description	SANYO mono-crystalline
Cell number	96
Cell type	Mono-crystalline
Cell size	156 × 156 mm
PV module dimension	1319 × 894 × 35 mm
Nominal power	180 W
Open circuit voltage V_{oc}	66.4 V
Short circuit current I_{sc}	3.65 A
Voltage V_{mpp}	54 V
Current I_{mpp}	3.33 A
Nominal operating temperature NOCT	45 ± 2°C
Temperature coefficient (P_{max})	-0.33%/°C
Temperature coefficient (I_{sc})	1.10 mA/°C
Temperature coefficient (V_{oc})	-0.173 V/°C

Table 2.
 PV modules characteristics.

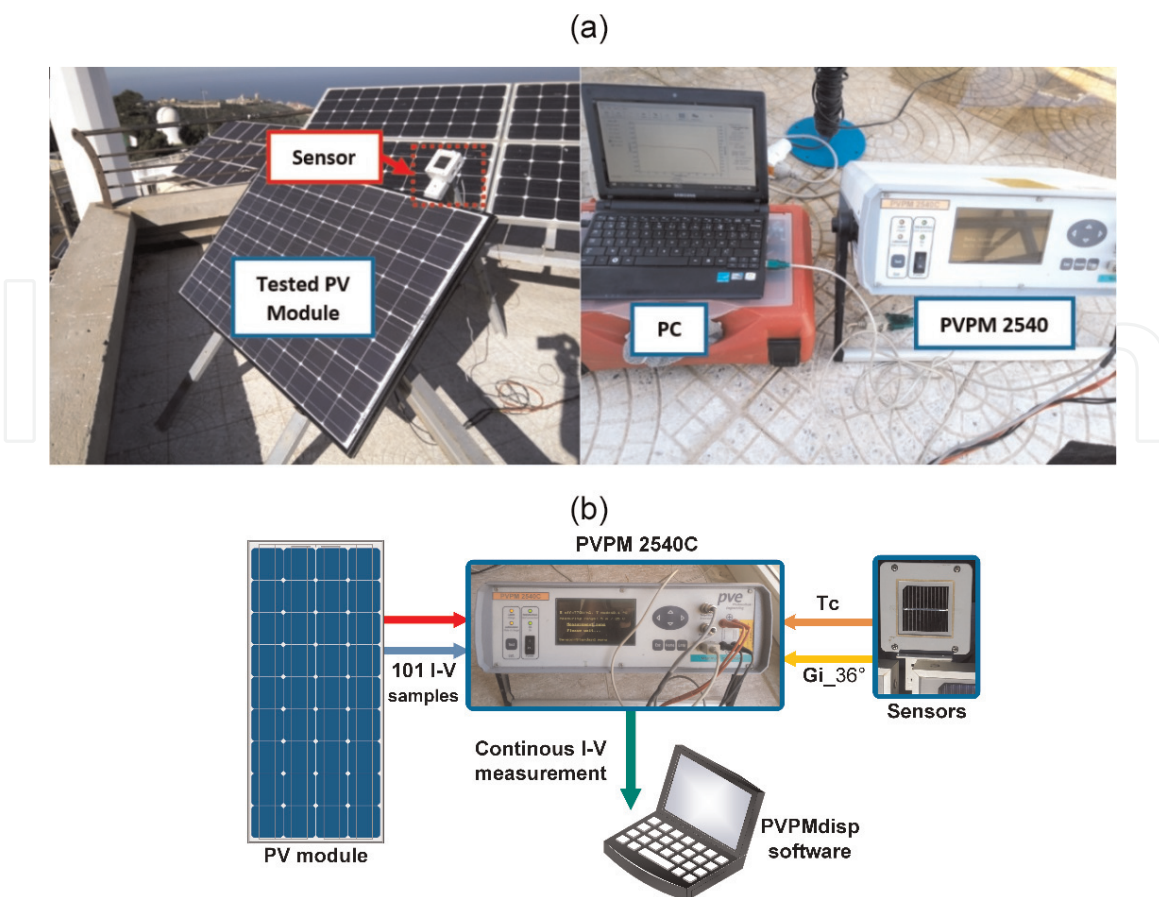


Figure 8.
 (a) Pictures for I-V experimental platform and (b) synoptic scheme for I-V measurement.

fall in the optimal solution. In the binary coding, the selected bit will change from 1 to 0 and vice versa as described in **Figure 7**. The mutation has low probability P_m in which, it will be affected for characters that correspond to $P_r < P_m$ in which, P_r is the drawing probability (randomly generated) [37, 38].

Our system is formed of mono-crystalline PV module SANYO technology with the characteristics listed in **Table 2**, peak measuring tracer and the necessary sensors. The experimental platform is illustrated in both **Figure 8a** and **b**.

After running of GA for 1000 cycles with the parameters listed in **Table 3** for both SDM and DDM using outdoor measurement of the systems, wherein extracted parameters are listed in **Table 4**. **Figure 9a** and **b** illustrate the agreement between the measured and simulated I(V) and P(V) characteristics for SDM model whose

GA parameters	Value
Number of cycle	1000
Population length	500
Crossover probability	0.7
Mutation probability	0.2

Table 3.
The GA parameters.

The electrical parameter	I_{ph} [A]	I_0 [A]	n	R_s [Ω]	R_{sh} [K Ω]
The identified value	3.0195	49591e-005	1.874*96	0.3273	8.1514

Table 4.
The obtained parameters for SDM.

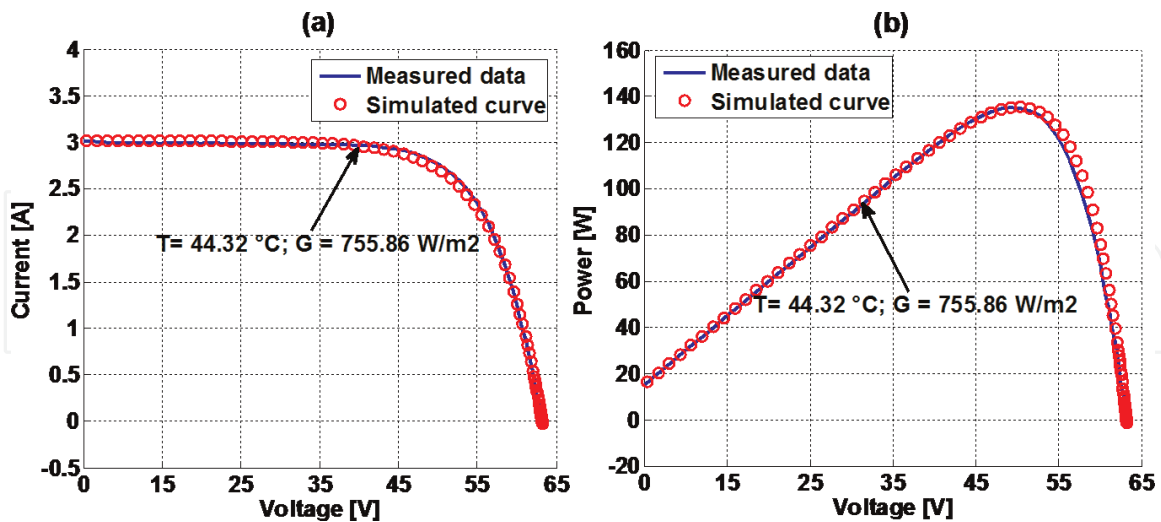


Figure 9.
Matching between measured and simulated characteristics for SDM. (a) I(V) and (b) P(V).

The electrical parameter	I_{ph} [A]	I_{01} [A]	I_{02} [A]	n_1	n_2	R_s [Ω]	R_{sh} [K Ω]
The identified value	3.0289	6.1035e-005	3.8147-006	1.3658*96	1.9179*96	0.1017	5.992

Table 5.
The obtained parameters for DDM.

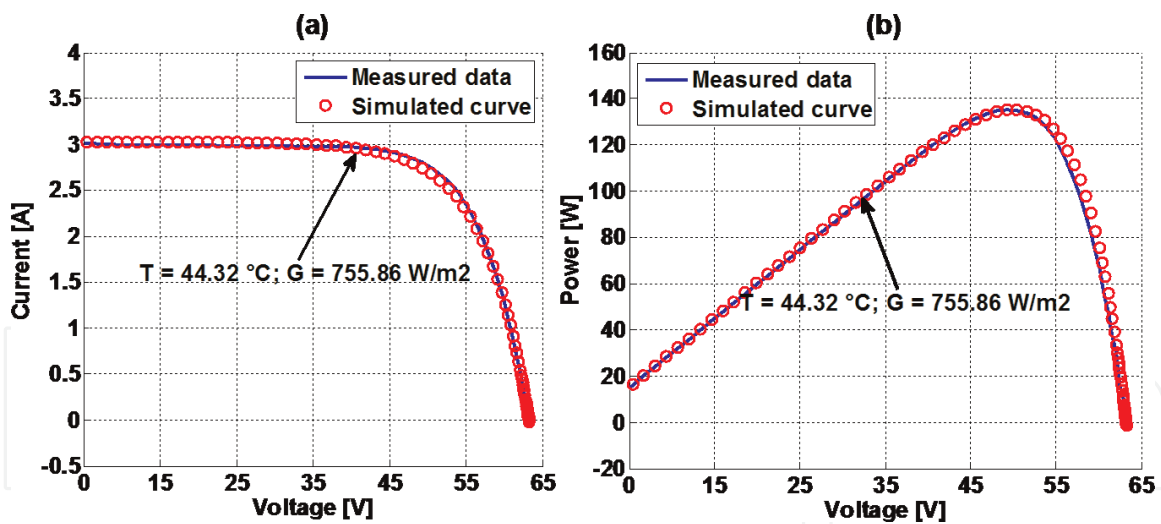


Figure 10.
 Matching between measured and simulated characteristics for DDM. (a) $I(V)$ and (b) $P(V)$.

E	ΔE					
	<i>NS</i>	<i>NL</i>	<i>ZE</i>	<i>PL</i>	<i>PS</i>	
<i>NS</i>	<i>PS</i>	<i>PS</i>	<i>PL</i>	<i>PS</i>	<i>PS</i>	
<i>NL</i>	<i>PS</i>	<i>PL</i>	<i>PL</i>	<i>PL</i>	<i>PS</i>	
<i>ZE</i>	<i>NL</i>	<i>NL</i>	<i>ZE</i>	<i>PL</i>	<i>PL</i>	
<i>PL</i>	<i>NS</i>	<i>NL</i>	<i>NL</i>	<i>NL</i>	<i>NS</i>	
<i>PS</i>	<i>NS</i>	<i>NS</i>	<i>NL</i>	<i>NS</i>	<i>NS</i>	

Table 6.
 The inference table.

obtained parameters are summarized in **Table 5**. **Figure 10a** and **b** show the agreement between the measured and simulated $I(V)$ and $P(V)$ characteristics for DDM model whose extracted parameters are summarized in **Table 6**.

Some parameters will be identified again in the dynamic study including the parameters involved in I_0 and I_{ph} equations, while the remaining will be adjusted to give more accuracy under variable weather conditions.

4. Dynamic parameters extraction of PV module

In this section, dynamic parameters identification will be described wherein the process is done by using 1 day profile of measurement. This allows to improve the nominal values given by the manufacturer, which can cause a significant error due to operating conditions and the consumed lifetime. Moreover, parameters obtained by static method can be adjusted by dynamic identification. For this end, automatic parameters adjustment using Levenberg-Marquardt optimization algorithm is employed.

As illustrated in **Figure 11**, the main idea is to take both PV module model and the MPPT as a single system with three outputs namely, I_{mpp} , V_{mpp} , and P_{mpp} . These outputs will be compared with 1 day profile of outdoor measurements. The process consists in minimizing the error between the model outputs and the real data. The whole system has been implemented in Matlab/Simulink tool.

For Sandia model, the process is carried out without the use of MPPT considering that this model has been established to the dynamic forecasting.

4.1 The MPPT used

An Accurate fuzzy logic MPPT algorithm is employed in our system (for SDM and DDM) in order to get satisfactory results in terms of precision and accuracy.

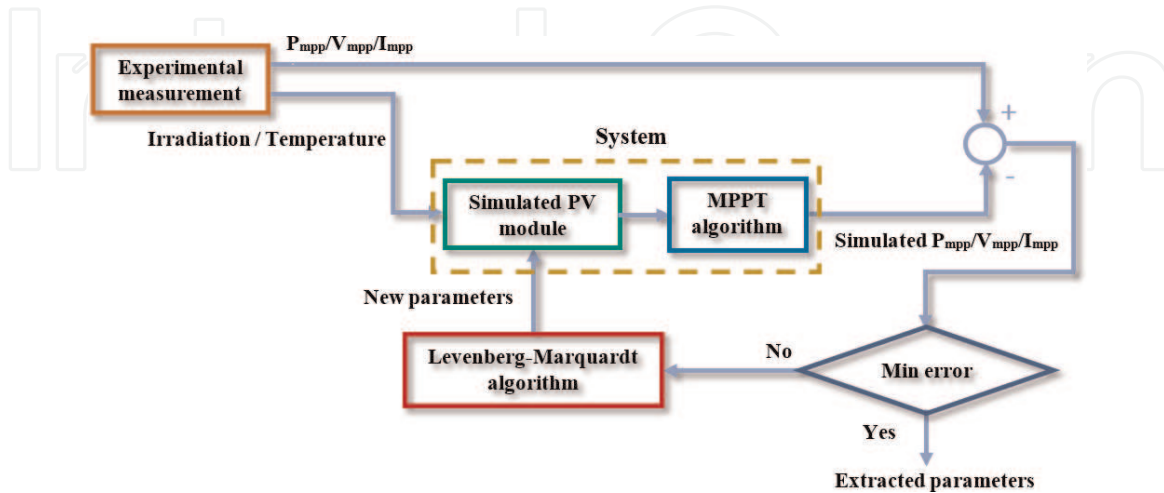


Figure 11. Dynamic parameters extraction process.

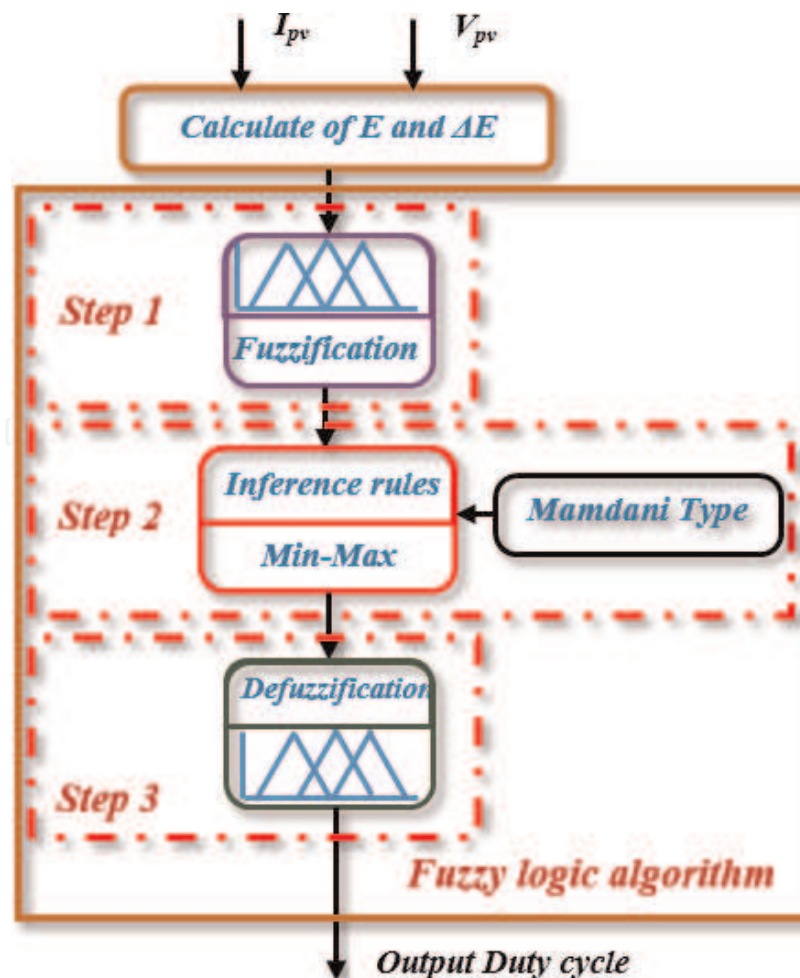


Figure 12. Fuzzy logic algorithm steps.

The algorithm is used to control a DC/DC boost converter for the purpose to keep the PV module working at the maximum point of power. Mamdani inference model is used with two inputs namely, the error E and the variation of the error ΔE . The calculation of these attributes is expressed in Eqs. (27)–(30).

$$\Delta P_{pv}(n) = P_{pv}(n) - P_{pv}(n - 1) \quad (27)$$

$$\Delta V_{pv}(n) = V_{pv}(n) - V_{pv}(n - 1) \quad (28)$$

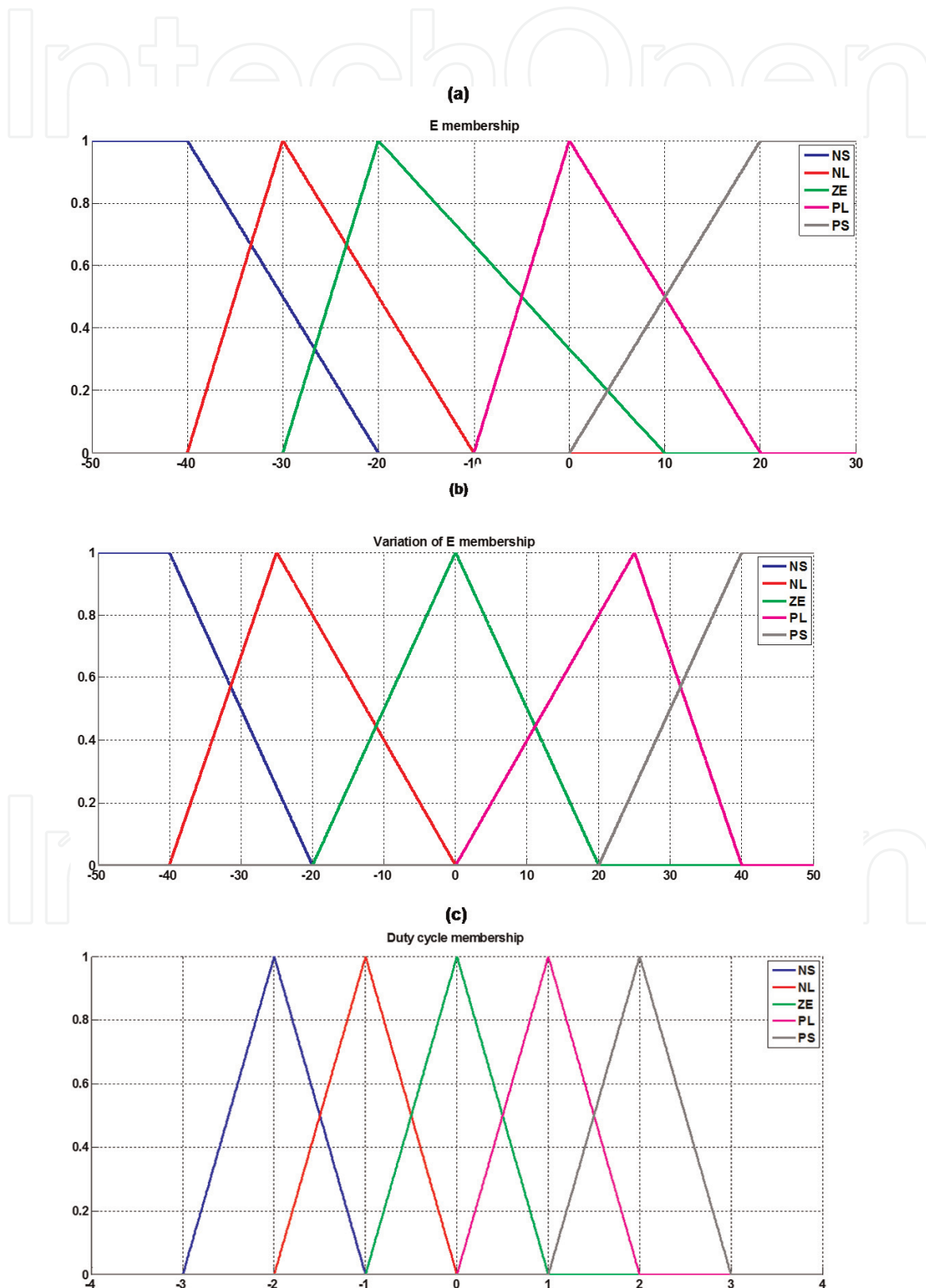


Figure 13. (a) Error membership; (b) variation of error membership; and (c) duty cycle membership.

$$E(n) = \frac{\Delta P_{pv}(n)}{\Delta V_{pv}(n)} \quad (29)$$

$$\Delta E(n) = E(n) - E(n - 1) \quad (30)$$

Three steps can characterize the fuzzy algorithm; the first one is the fuzzification process that consists on the conversion of the numerical inputs values (E and ΔE) into linguistic values by the substitution in the membership functions. The second step is the inference process, which is considered as the main stage in the fuzzy algorithm wherein the relation between the inputs and the output is done. The third step is the defuzzification where the process converts the linguistic decision into numerical output. **Figure 12** describes briefly the fuzzy processing steps [39].

SDM parameters	Boundaries	DDM parameters	Boundaries	Sandia parameters	Boundaries
n	[0, 2]*96	n_1, n_2	[0, 2]*96	C_0	[0, 2]
R_s [Ω]	[0, 1]	R_s [Ω]	[0, 1]	C_1	[-1, 1]
R_{sh} [Ω]	[0, 10 ⁴]	R_{sh} [Ω]	[0, 10 ⁴]	C_2	[-10, 10]
E_{g0}	[0, 1]	E_{g01-2}	[0, 2]	C_3	[-10, 50]
A	[0, 1]	α_{1-2}	[0, 1]	α_{imp} [°C ⁻¹]	[0, 1]
B	[0, 10 ⁴]	β_{1-2}	[0, 10 ⁴]	β_{Vmp} [V/°C]	[-1, 0]
μ	[0, 1]	μ	[0, 1]	n	
I_{sc}	[3, 3.7]	I_{sc}	[3, 3.7]		
V_{oc}	[60, 66.8]	V_{oc}	[60, 66.8]		

Table 7.
Lower and upper boundaries selected for each model parameters.

SDM parameters	Values	DDM parameters	Values	Sandia parameters	Values
n	105.73/96	n_1, n_2	90.73/96; 73.39/96	C_0	1.058
R_s [Ω]	0.82495	R_s [Ω]	0.3219	C_1	0.020
R_{sh} [Ω]	8.371 × 10 ³	R_{sh} [Ω]	4.9664 × 10 ³	C_2	-0.341
E_{g0} [ev]	1.4525	E_{g01-2} [ev]	1.649; 1.31	C_3	-9.997
α	6.56 × 10 ⁻⁴	α_{1-2}	0.0018; 0.0132	α_{imp} [°C ⁻¹]	2.53 × 10 ⁻¹⁴
β	126.11	β_{1-2}	694.84; 1020.76	β_{Vmp} [V/°C]	-0.203
μ	0.0121	μ	0.0112	n	1.221
I_{sc}	3.671	I_{sc}	3.629		
V_{oc}	66.208	V_{oc}	65.527		

Table 8.
Dynamic extracted parameters.

For both inputs and output, five trapezoidal and triangular membership functions have been employed namely: NS (negative strong), NL (negative low), ZE (zero), PL (positive low) and PS (positive strong). The center of gravity based method is used for the defuzzification to provide the control duty cycle after applying the Mamdani inference model given in **Table 6**. **Figure 13a, b and d** describes the used membership functions [39].

4.2 Simulation study

The Levenberg-Marquardt algorithm is implemented using 1 day profile of outdoor real measurement of dynamic PV outputs (P_{mpp} , I_{mpp} and V_{mpp}). The process consists in minimizing the error between simulated outputs of both SDM and DDM and 8 h of real data (09:00 am–05:00 pm). The peak measuring device tracer (PVPM 2540C) has been programmed to provide 1 sample per minute. **Table 7** lists the lower and upper limits search of the extracted parameters. The extracted parameters using the dynamic method are summarized in **Table 8**. The inputs measurement of the irradiation and the temperature are illustrated in **Figure 14a and b**, respectively. Satisfactory results have been obtained in terms of matching between the real data and the simulated outputs P_{mpp} , I_{mpp} and V_{mpp} for SDM, DDM and Sandia as shown in **Figure 15a–c**, respectively.

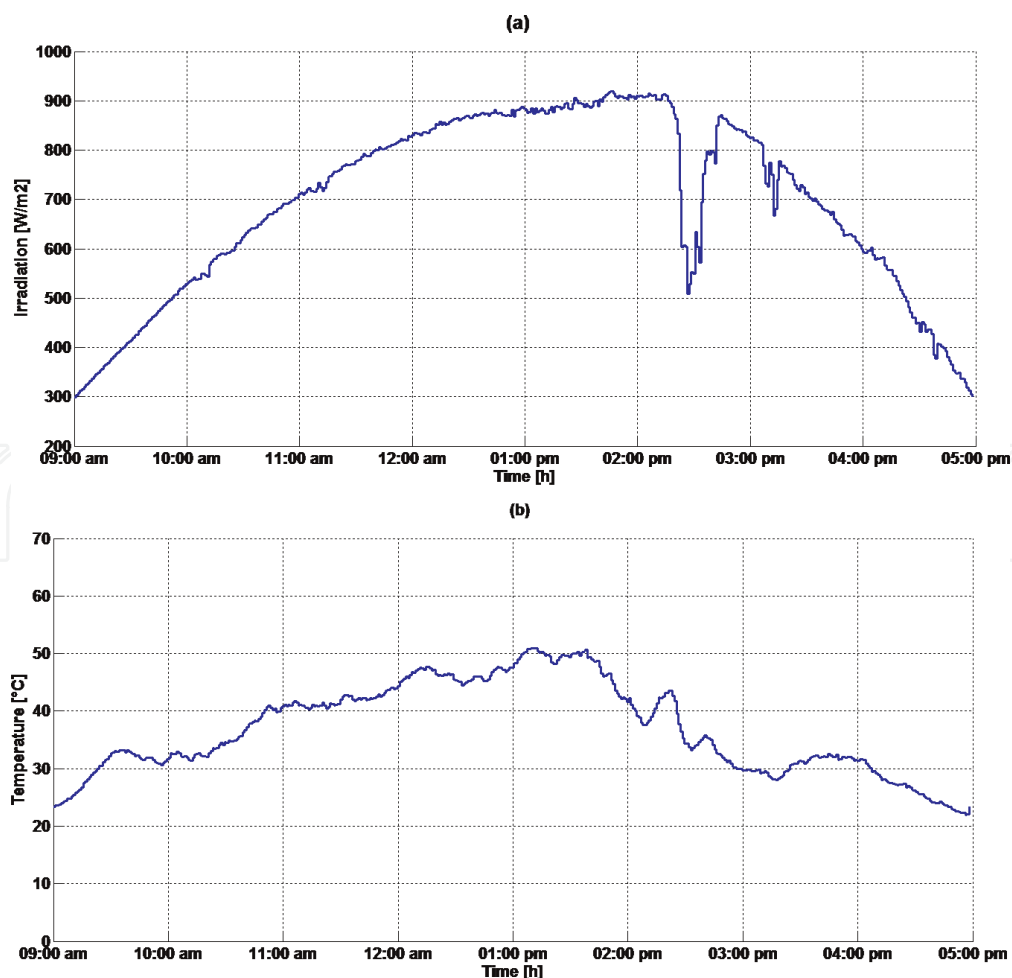


Figure 14. Eight hours profile (09:00 am–05:00 pm). (a) Irradiation and (b) temperature.

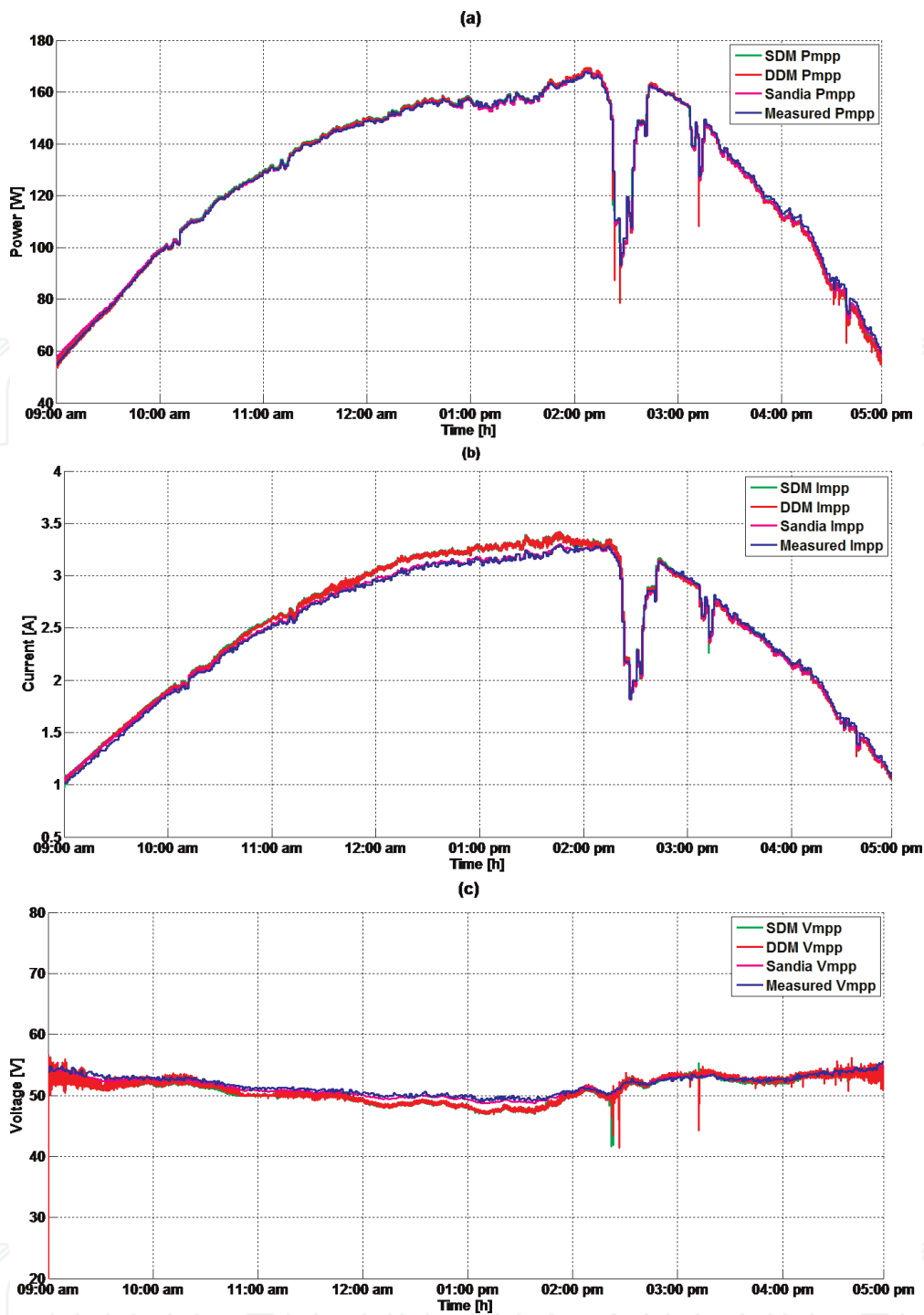


Figure 15. Eight hours profile (09:00 am–05:00 pm) of: measured output VS obtained output for SANYO mono-crystalline. (a) Measured P_{mpp} vs obtained P_{mpp} from: SDM, DDM and Sandia, (b) measured I_{mpp} vs obtained I_{mpp} from: SDM, DDM and Sandia and (c) measured V_{mpp} VS obtained V_{mpp} from: SDM, DDM and Sandia.

5. Experimental validation

In this section, a validation with an unseen data is carried out to test and compare the effectiveness of the proposed enhancement. The three developed models will be compared with real measurement profile (09:00 am–05:00 pm) of irradiation and temperature for different weather conditions. Wherein, the SDM and DDM models using the developed parameters are compared with the former nominal parameters listed in **Table 9**, Sandia model and the real data. Three different skies of real measurement have been used for this validation namely, clear day,

Parameters	Value
E_{g0}	1.16 eV
α	4.73×10^{-4}
β	1000
μ	1.10 mA/°C
I_{sc}	3.65 A
V_{oc}	66.4 V

Table 9.
Nominal parameters.

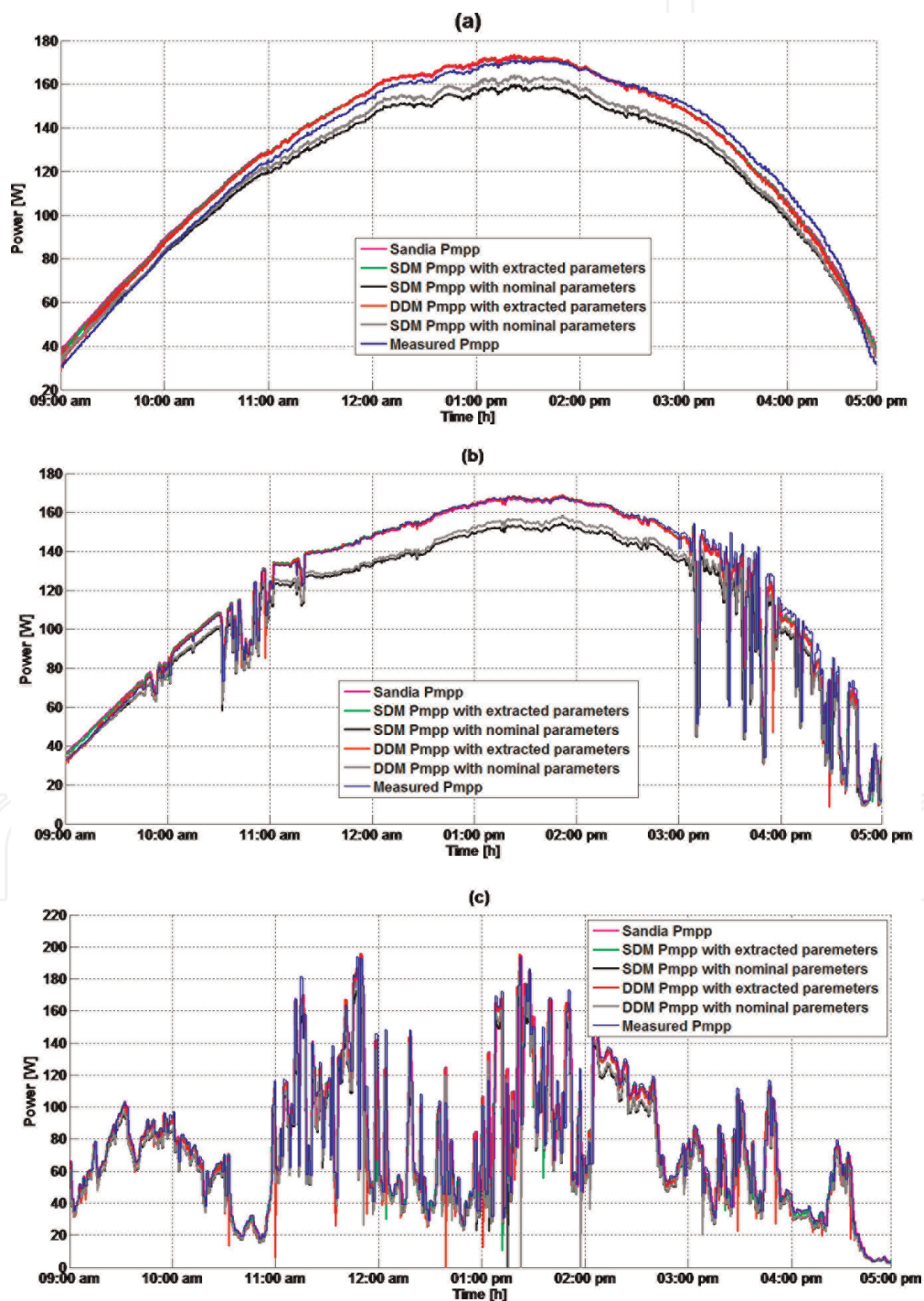


Figure 16.
Eight hours profile (09:00 am–05:00 pm) of: measured P_{mpp} vs obtained P_{mpp} from: SDM, SDM with nominal parameters, DDM, DDM with nominal parameters and Sandia. (a) clear day, (b) semi-cloudy day and (c) cloudy day.

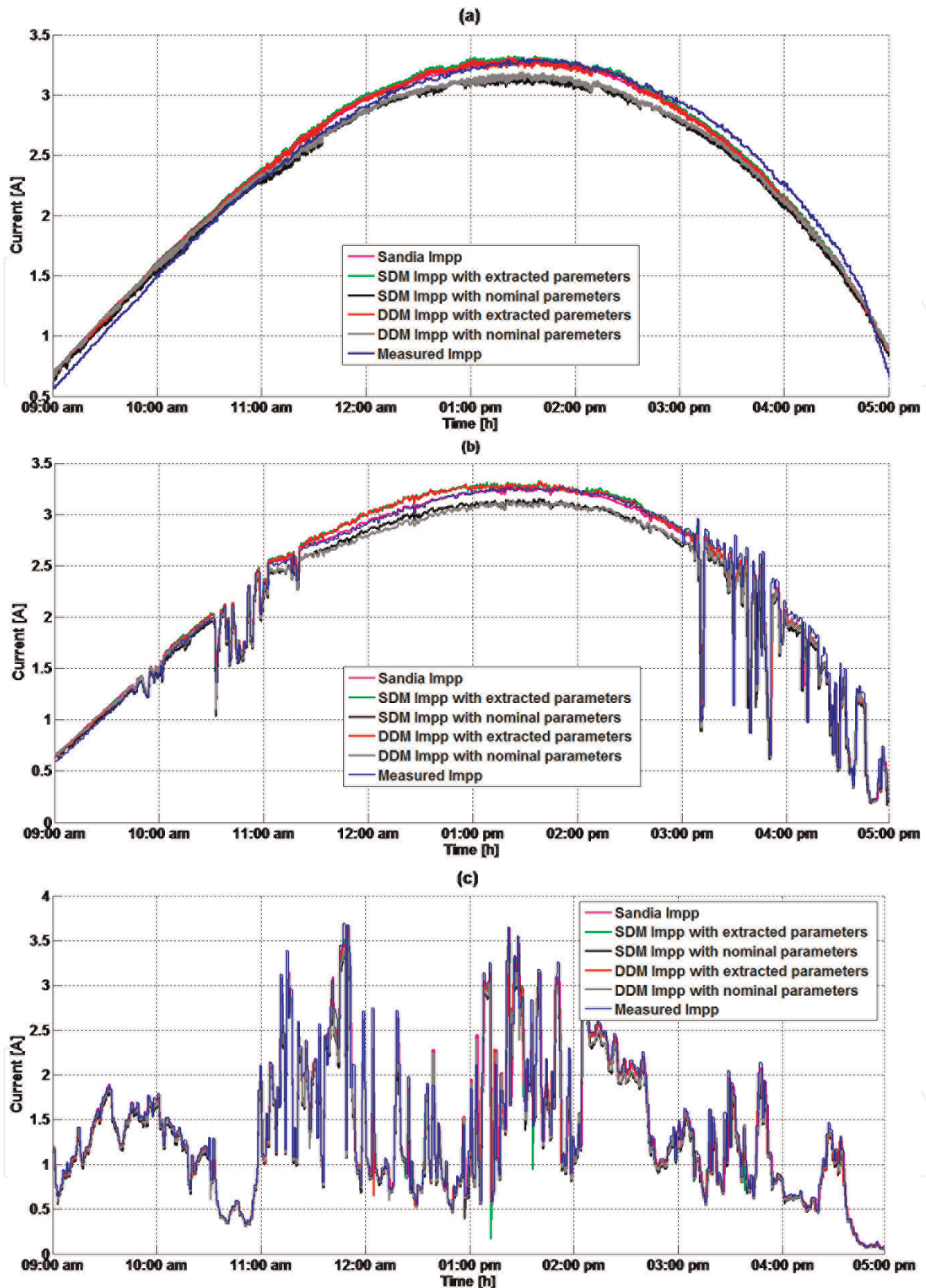


Figure 17. Eight hours profile (09:00 am–05:00 pm) of: measured I_{mpp} vs obtained I_{mpp} from: SDM, SDM with nominal parameters, DDM, DDM with nominal parameters and Sandia. (a) clear day, (b) semi-cloudy day and (c) cloudy day.

semi-cloudy day and cloudy day. The matching in the power (P_{mpp}) between and the real data and SDM and DDM with nominal parameters, SDM and DDM with the new parameters and Sandia model is illustrated in **Figure 16a–c** for clear day, semi-cloudy day and cloudy day respectively. Besides, the agreement in the voltage and the current (V_{mpp} and I_{mpp}) for these models with the real data is shown in **Figure 17a–c** and **Figure 18a–c**, respectively.

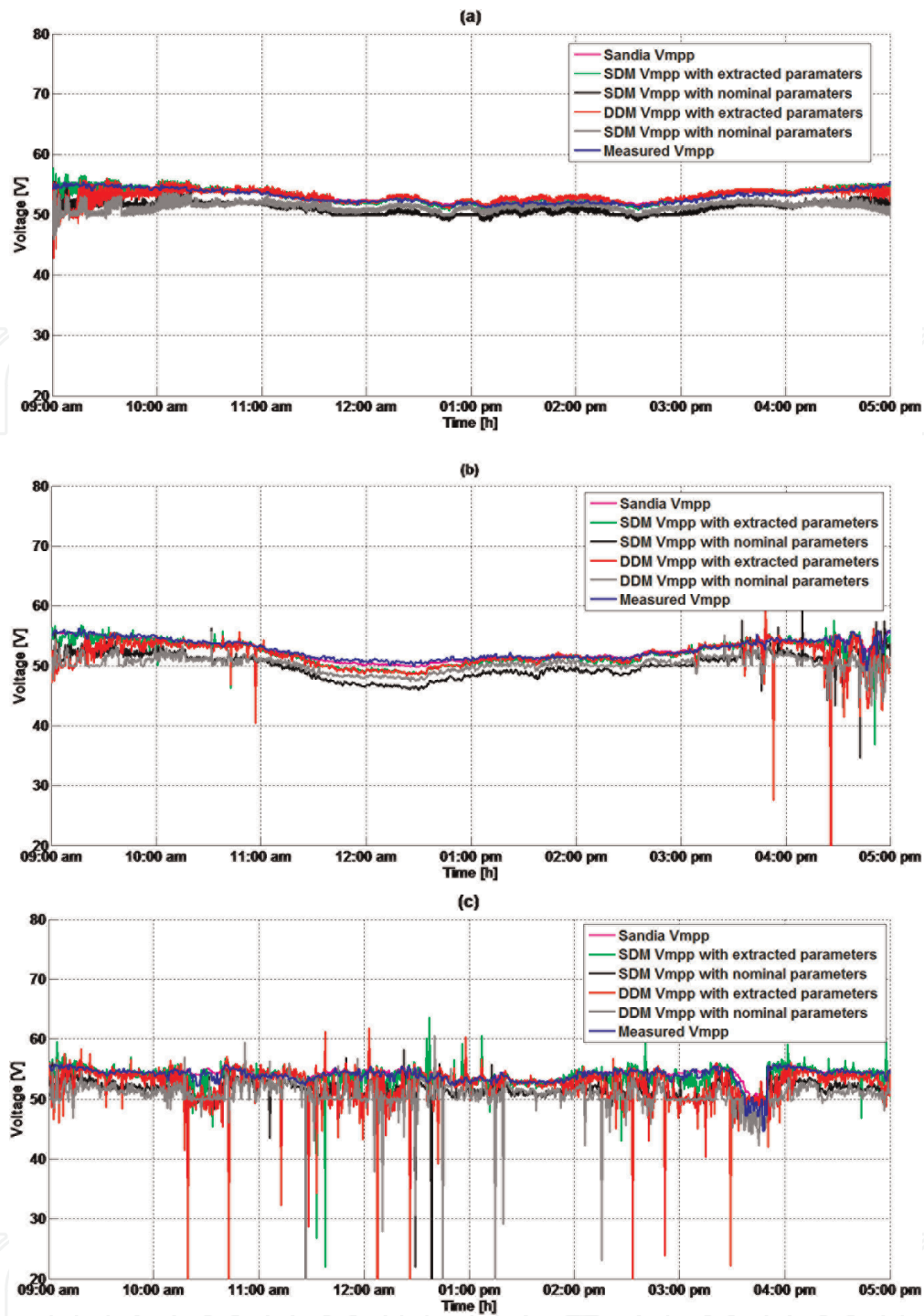


Figure 18. Eight hours profile (09:00 am–05:00 pm) of: measured V_{mpp} vs obtained V_{mpp} from: SDM, SDM with nominal parameters, DDM, DDM with nominal parameters and Sandia. (a) clear day, (b) semi-cloudy day and (c) cloudy day.

It is clearly found that an improved agreement has been shown by models with new parameters compared to that given by the nominal parameters and the static method.

For more clarity, the hourly power efficiency given by the presented models and the real data has been calculated. It consists on the average of the power during 1 h versus the optimal PV module power (Eq. (31)) [40].

$$\text{Hourly efficiency} = \frac{\sum_{k=1}^N P_{MPP}(k)/N}{P_{PV_optimal}} \quad (31)$$

in which, N is the number samples per hour.

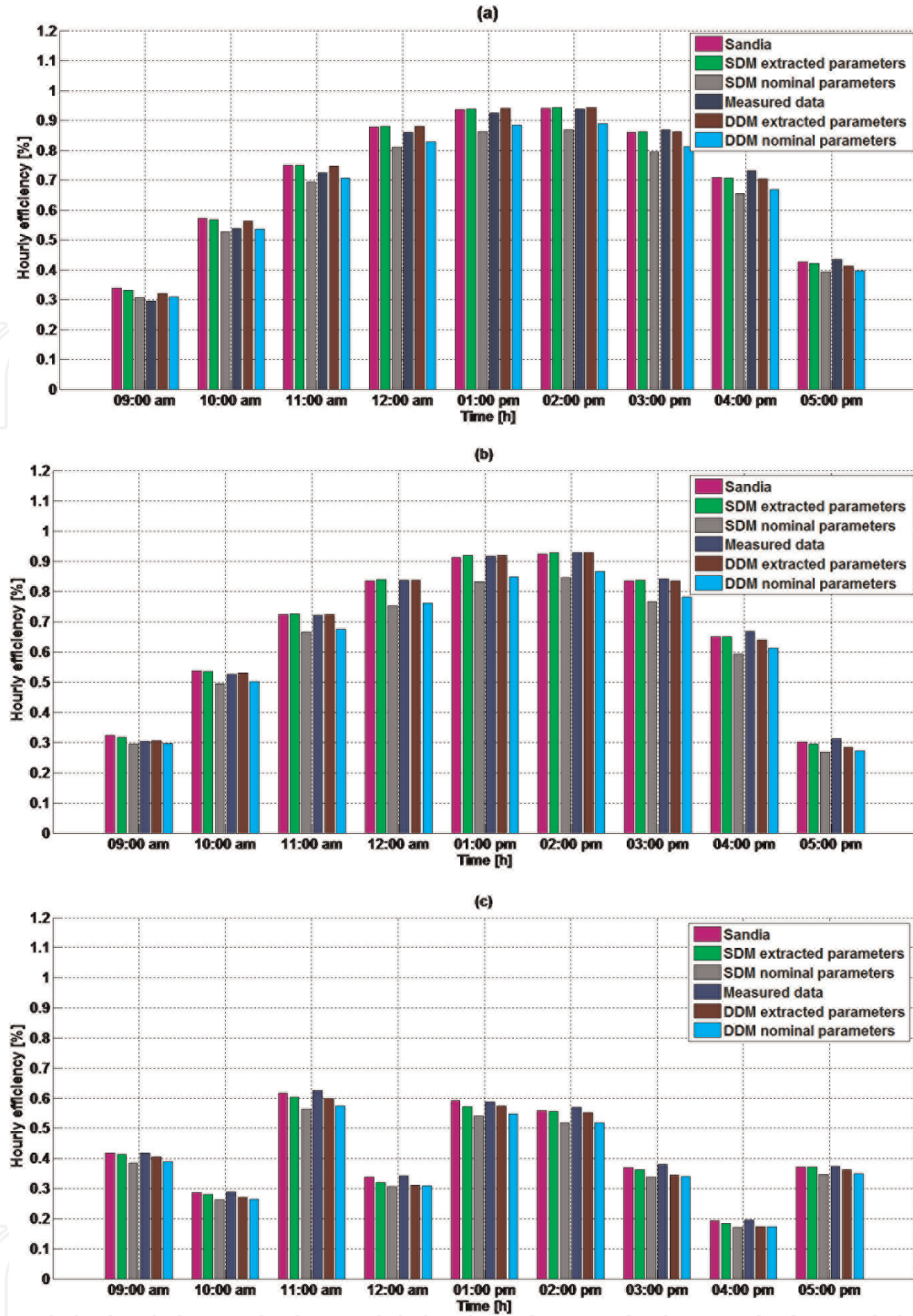


Figure 19. Eight hours profile (09:00 am–05:00 pm) of: measured hourly efficiency vs obtained hourly efficiency from: SDM, SDM with nominal parameters, DDM, DDM with nominal parameters and Sandia. (a) Clear day, (b) semi-cloudy day, and (c) cloudy day.

Figure 19a–c show the bar-graph of the hourly power efficiency of the proposed models for the three weather conditions, namely the clear day, semi-cloudy day and cloudy day, respectively. The enhanced models present higher hourly power efficiency versus models with the former parameters and those given by the static error technique. Furthermore, root mean square error (RMS) and the mean absolute error (MAE) between the real data and the studied models are calculated by Eqs. (19) and (32) to show the enhancement of the proposed method.

$$MAE = \frac{1}{N} \sum_{i=1}^N \frac{|Simulated\ output - Measured\ output|}{Measured\ output} \quad (32)$$

Day	Weather	Error [%]	Current					Voltage				
			SDM	SDMnp	DDM	DDMnp	Sandia	SDM	SDMnp	DDM	DDMnp	Sandia
22/01/2018	Clear day	RMS	0.72	1.12	0.69	0.93	0.68	1.48	2.21	1.63	2.34	1.49
		MAE	4.31	5.05	4.24	5.12	4.38	1.27	4.07	1.77	3.70	1.17
29/01/2018	Semi-cloudy	RMS	0.22	0.45	0.24	0.32	0.23	3.30	9.10	6.53	7.87	1.13
		MAE	3.14	5.40	2.96	4.35	2.85	1.50	5.34	2.37	4.76	0.57
28/01/2018	Cloudy day	RMS	0.43	0.48	0.47	0.31	0.52	9.05	8.77	12.2	12.3	1.83
		MAE	4.38	6.62	5.02	3.93	5.60	2.06	4.63	4.05	6.18	0.77
Day	Weather	Error [%]	Power									
22/01/2018	Clear day	RMS	3.65	8.49	3.45	4.34	3.79					
		MAE	4.24	6.79	3.74	4.44	4.51					
29/01/2018	Semi-cloudy	RMS	2.48	4.30	2.48	4.30	0.82					
		MAE	5.14	11.7	4.58	10.3	2.33					
28/01/2018	Cloudy day	RMS	5.35	4.82	5.51	5.24	2.79					
		MAE	1.37	1.56	1.55	1.57	5.63					

Table 10.
 Calculated RMS (%) and MAE (%).

where N is the number of samples [41].

The aforementioned results show clearly that the extracted parameters of the PV module using dynamic techniques present more accuracy compared with the static method and the parameters given by the manufacturer. Indeed, the parameters obtained by the static method are clearly improved for variable weather conditions (irradiation and temperature), which is confirmed using different skies. **Table 10** summarizes the calculated RMS and MAE errors values which show obviously that the developed models present advantages comparing with real outdoor data of different weather conditions.

6. Conclusion

In this chapter, both dynamic and static parameters identification methods have been highlighted and compared with real measurement. The SDM and DDM nominal parameters involved in I_0 and I_{ph} equations have been developed by dynamic method. This improved result has been compared with that given by the static technique and Sandia model versus out-door real data for different skies (clear day, semi-cloudy day and cloudy day). It was found that SDM and DDM based on the parameters extracted by dynamic method give satisfactory accuracy, which is confirmed by some calculated indicator such as: the hourly efficiency and both root mean square error (RMS) and the mean absolute error (MAE). This allows to solve modeling problems of PV module that apply for several applications such as fault detection.

IntechOpen

Author details

Sid-Ali Blaifi^{1,2*} and Bilal Taghezouit³


1 Research Laboratory of Electrical Engineering and Automatic LREA, University of Medea, Medea, Algeria

2 Department of Science and Technologies, University of Khemis Miliana, Algeria

3 Centre de Développement des Energies Renouvelables, CDER, Algiers, Algeria

*Address all correspondence to: sidali.blaifi@gmail.com; s.blaifi@univ-dbk.m.dz

IntechOpen

© 2020 The Author(s). Licensee IntechOpen. Distributed under the terms of the Creative Commons Attribution - NonCommercial 4.0 License (<https://creativecommons.org/licenses/by-nc/4.0/>), which permits use, distribution and reproduction for non-commercial purposes, provided the original is properly cited. 

References

- [1] AbdulHadi M, Al-Ibrahim AM, Virk GS. Neuro-fuzzy-based solar cell model. *IEEE Transactions on Energy Conversion*. September 2004;**19**(3): 619-624
- [2] Mekki H, Mellit A, Salhi H, Khaled B. Modeling and simulation of photovoltaic panel based on artificial neural networks and VHDL-language. In: *Electronics, Circuits and Systems, 2007. ICECS 2007. 14th IEEE International Conference*.
- [3] Mellit A, Saglam S, Kalogirou SA. Artificial neural network-based model for estimating the produced power of a photovoltaic module. *Renewable Energy*. 2013;**60**:71-78
- [4] Askarzadeh A. Voltage prediction of a photovoltaic module using artificial neural networks. *International Transactions on Electrical Energy Systems*. 2014;**24**:1715-1725
- [5] Ortiz-Rivera EI, Peng FZ. Analytical Model for a Photovoltaic Module Using the Electrical Characteristics provided by the Manufacturer Data Sheet Power Electronics Specialists Conference. PESC '05. IEEE 36th. 2005
- [6] King DL, Boyson WE, Kratochvil JA. Photovoltaic array performance model. Sandia Report No. SAND 2004-3535. 2004. Available from: <http://www.sandia.gov/pv/docs/PDF/King%20SAND.pdf>
- [7] Zhou W, Yang H, Fang Z. A novel model for photovoltaic array performance prediction. *Applied Energy*. 2007;**84**:1187-1198
- [8] Deline C, Dobos A, Janzou S, Meydbray J, Donovan M. A simplified model of uniform shading in large photovoltaic arrays. *Solar Energy*. 2013;**96**:274-282
- [9] Chenni R, Makhlouf M, Kerbache T, Bouzid A. A detailed modeling method for photovoltaic cells. *Energy*. 2007;**32**: 1724-1730
- [10] Rosell JI, Ibanez M. Modelling power output in photovoltaic modules for outdoor operating conditions. *Energy Conversion and Management*. 2006;**47**:2424-2430
- [11] Castaner L, Silvestre S. Front matter. In: Castaner RL, Silvestre S, editors. *Modeling Photovoltaic Systems Using PSpice*. Chichester, England: Wiley; 2003. p. 376
- [12] Ishaque K, Salam Z, Taheri H, Shamsudin A. A critical evaluation of EA computational methods for photovoltaic cell parameter extraction based on two diode model. *Solar Energy*. 2011;**85**:1768-1779
- [13] Easwarakhanthan T, Bottin J, Bouhouch I, Boutrit C. Nonlinear minimization algorithm for determining the solar cell parameters with microcomputers. *International Journal of Solar Energy*. 1986;**4**:1-12
- [14] Dkhichi F, Oukarfi B, Fakkar A, Belbounaguia N. Parameter identification of solar cell model using LevenbergeMarquardt algorithm combined with simulated annealing. *Solar Energy*. 2014;**110**:781-788
- [15] El-Naggar KM, AlRashidi MR, AlHajri MF, Al-Othman AK. Simulated annealing algorithm for photovoltaic parameters identification. *Solar Energy*. 2012;**86**:266-274
- [16] AlHajri MF, El-Naggar KM, AlRashidi MR, Al-Othman AK. Optimal extraction of solar cell parameters using pattern search. *Renewable Energy*. 2012;**44**:238-245
- [17] Chen Z, Wu L, Lin P, Wu Y, Cheng S. Parameters identification of

photovoltaic models using hybrid adaptive Nelder-Mead simplex algorithm based on eagle strategy. *Applied Energy*. 2016;**182**:47-57

[18] Hamid NFA, Rahim NA, Selvaraj J. Solar cell parameters identification using hybrid Nelder-Mead and modified particle swarm optimization. *Journal of Renewable and Sustainable Energy*. 2016;**8**. DOI: 10.1063/1.4941791

[19] Jervase JA, Bourdoucen H, Al-Lawati A. Solar cell parameter extraction using genetic algorithms. *Measurement Science and Technology*. 2001;**12**(11):1922

[20] Huang W, Jiang C, Xue L, Song D. Extracting solar cell model parameters based on chaos particle swarm algorithm. In: 2011 International Conference on Electric Information and Control Engineering. Vol. 2011. pp. 398-402

[21] Meiyong Y, Xiaodong W, Yousheng X. Parameter extraction of solar cells using particle swarm optimization. *Journal of Applied Physics*. 2009;**105**:094502-094508

[22] Hachana O, Hemsas KE, Tina GM, Ventura C. Comparison of different metaheuristic algorithms for parameter identification of photovoltaic cell/module. *Journal of Renewable and Sustainable Energy*. 2013;**5**:053122

[23] Ma J, Man KL, Guan SU, Ting TO, Wong PWH. Parameter estimation of photovoltaic model via parallel particle swarm optimization algorithm. *International Journal of Energy Research*. 2016;**40**: 343e352

[24] Jordehi AR. Time varying acceleration coefficients particle swarm optimization (TVACPSO): A new optimization algorithm for estimating parameters of PV cells and modules.

Energy Conversion and Management. 2016;**129**:262-274

[25] Muralidharan R. Parameter extraction of solar photovoltaic cells and modules using current-voltage characteristics. *International Journal of Ambient Energy* (2016). *Europe-China cooperation and competition in the Green Industries*; 2017;**38**(5):509-513. DOI: 10.1080/01430750. 2016.1144525

[26] Oliva D, Cuevas E, Pajares G. Parameter identification of solar cells using artificial bee colony optimization. *Energy*. 2014;**72**:93-102

[27] Ma J, Ting TO, Man KL, Zhang N, Guan S-U, Wong PWH. Parameter estimation of photovoltaic models via Cuckoo search, Hindawi Publish. Corporat. *Journal of Applied Mathematics*. 2013;**362619**. 8 pages

[28] Jamadi M, Merrikh-Bayat F, Bigdeli M. Very accurate parameter estimation of single- and double-diode solar cell models using a modified artificial bee colony algorithm. *International Journal of Energy and Environmental Engineering*. 2016;**7**: 13-25

[29] Askarzadeh A, Rezazadeh A. Artificial bee swarm optimization algorithm for parameters identification of solar cell models. *Applied Energy*. 2013;**102**:943-949

[30] Alam DF, Yousri DA, Eteiba MB. Flower pollination algorithm based solar PV parameter estimation. *Energy Conversion and Management*. 2015;**101**: 410-422

[31] Benkercha R, Moulahoum S, Colak I, Taghezouit B. PV module parameters extraction with maximum power point estimation based on flower pollination algorithm. In: 2016 IEEE International Power Electronics and Motion Control Conference, PEMC. 2016. pp. 442-449

- [32] Ram JP, Babu TS, Dragicevic T, Rajasekar N. A new hybrid bee pollinator flower pollination algorithm for solar PV parameter estimation. *Energy Conversion and Management*. 2017;**135**:463-476
- [33] Askarzadeh A, Rezaazadeh A. Parameter identification for solar cell models using harmony search-based algorithms. *Solar Energy*. 2012;**86**: 3241-3249
- [34] Han W, Wang H-H, Chen L. Parameters identification for photovoltaic module based on an improved artificial fish swarm algorithm. *Scientific World Journal*. 2014;**859239**. 12 pages
- [35] Kichou S, Silvestre S, Guglielminotti L, et al. Comparison of two PV array models for the simulation of PV systems using five different algorithms for the parameters identification. *Renewable Energy*. 2016; **99**:270-279
- [36] Blaifi S-a, Moulahoum S, Taghezouit B, Saim A. An enhanced dynamic modeling of PV module using Levenberg-Marquardt algorithm. *Renewable Energy*. 2019;**135**:745-760
- [37] Blaifi S, Moulahoum S, Colak I, Merrouche W. An enhanced dynamic model of battery using genetic algorithm suitable for photovoltaic applications. *Applied Energy*. 2016;**169**:888-898
- [38] Blaifi S, Moulahoum S, Colak I, Merrouche W. Monitoring and enhanced dynamic modeling of battery by genetic algorithm using LabVIEW applied in photovoltaic system. *Electrical Engineering*. June 2018;**100** (2):1021-1038
- [39] Blaifi S, Moulahoum S, Benkercha R, Taghezouit B, Saim A. M5P model tree based fast fuzzy maximum power point tracker. *Solar Energy*. 2018;**163**:405-442
- [40] Benyoucef AS et al. Artificial bee colony based algorithm for maximum power point tracking (MPPT) for PV systems operating under partial shaded conditions. *Applied Soft Computing*. 2015;**32**:38-48
- [41] Blaifi S, Moulahoum S, Colak I, Merrouche W. An enhanced dynamic model of battery using genetic algorithm suitable for photovoltaic applications. *Applied Energy*. 2016;**169**: 888-898